THE ASTRONOMICAL JOURNAL VOLUME 105, NUMBER 5 MAY 1993

THE PARKES–MIT–NRAO (PMN) SURVEYS. I. THE 4850 MHz SURVEYS AND DATA REDUCTION

MARK R. GRIFFITH

Department of Physics, Massachusetts Institute of Technology, Cambridge, Massachusetts 02139
Electronic mail: griffith@maggie.mit.edu

ALAN E. WRIGHT

Australia Telescope National Facility,[1] Parkes, New South Wales, Australia
Electronic mail: awright@atnf.csiro.au

Received 1992 October 6; revised 1992 December 21

ABSTRACT

We describe radio surveys covering the sky from $-87.5°$ to $+10°$ declination made using the Parkes 64 m radio telescope with the NRAO multibeam receiver at a frequency of 4850 MHz during 1990. We have fully reduced the data from the Southern Survey ($-87.5°<\delta<-37°$) and Tropical Survey ($-29°<\delta<-9.5°$). Together, these surveys cover 4.51 sr and contain 36 640 sources to a flux limit that is, typically, about 35 mJy but varies as a function of declination. They increase the number of known sources in the regions surveyed by approximately a factor of 5. In this paper, we describe the overall PMN Surveys, the data reduction techniques adopted, and assess the data quality of the two lists of sources resulting from the Southern and Tropical Surveys.

I. INTRODUCTION

The large-area continuum radio surveys are the foundation upon which all other radio astronomy rests. They provide the catalogs from which astronomers draw radio sources to study in more detail, as well as the objects with which to calibrate the positional and flux density accuracy of their instruments.

In the Southern Hemisphere, the major all-sky surveys have been those made with the Molonglo Cross instrument at 408 MHz (Large *et al.* 1981) and the 2700 MHz survey made with the Parkes 64 m reflector (see, for example, Bolton *et al.* 1979).

Until recently, large-area surveys at frequencies higher than 2700 MHz were difficult to make because small telescope beamwidths and relatively high receiver system temperatures implied prohibitively large amounts of observing time. In the last few years, however, receiver technology, the accurate control of large single-dish telescopes, and the advent of multibeam receiving systems have allowed large-area, high-frequency surveys to be made quickly.

The principal institutions involved in the new surveys were the Parkes Radio Observatory of the Australia Telescope National Facility (ATNF); the Massachusetts Institute of Technology (MIT); and the National Radio Astronomy Observatory (NRAO), hence the name PMN, from the initial letters of these institutions.

The primary goal of the new PMN Surveys described here was to provide a new high quality catalog of radio sources for the Southern Hemisphere. The secondary goal was to complement the Northern Hemisphere 4850 MHz survey of Condon *et al.* (1989) and the resulting source catalog (Gregory & Condon 1991).

Condon *et al.*'s northern survey was made using the NRAO 91 m telescope for the declination range $+75°$ to $0°$, and the NRAO 140 ft (43 m) telescope for the range $+5°$ to $-40°$ (Condon *et al.* 1991). However, using the smaller telescope for the southern parts of the Condon surveys means that the flux limit is not as deep as that of the northern survey.

The PMN Surveys extend the 4850 MHz survey to the Southern Hemisphere with approximately the same sensitivity as that of the 91 m survey. The new surveys also partly supersede and partly complement the existing large-area southern surveys observed at lower frequencies. A preliminary account of this work has been given by Griffith *et al.* (1991). For a more detailed description of the information given below, see Griffith's Ph.D. thesis (1993).

2. EQUIPMENT

2.1 Telescope and Receivers

The Parkes radio telescope is a 64 m altitude–azimuth mounted paraboloid. It is located close to longitude 148.25° east and latitude 33.00° south near the town of Parkes in NSW, Australia. At the frequency used in the PMN Surveys (4850 MHz), the whole of the dish surface forms an effective reflector and the "S/T" ratio is close to 2.0 Jy/K.

For the PMN Surveys, we used a 4850 MHz multibeam receiving system built specifically for the Northern Hemisphere surveys. (For a detailed description see Condon *et al.* 1989). The only major difference from the system described by Condon *et al.* is that the receiver has been upgraded to use low-noise high electron mobility transistor (HEMT) amplifiers in each channel. For our survey, each channel had a typical system temperature of about 40 K and a bandwidth of 600 MHz centered on 4850 MHz.

The receiver's 14 channels were fed in pairs from seven beams. The beams were arranged in a filled hexagon pat-

[1]The Australia Telescope National Facility is operated in association with the Division of Radiophysics by CSIRO.

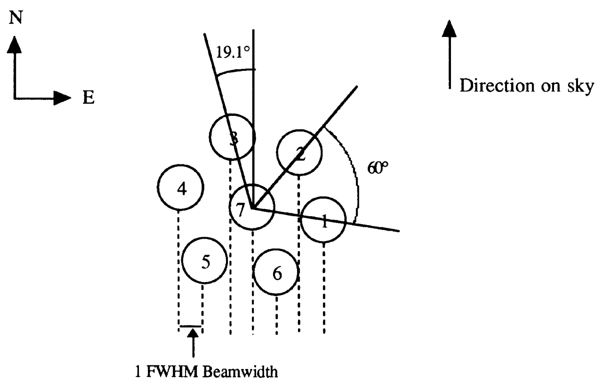

FIG. 1. Orientation of the 4850 MHz receiver on the sky during the PMN Surveys. If the receiver is rotated to an angle of 19.1° to the direction of motion as shown, the tracks will be nearly uniformly separated by one FWHM beamwidth.

tern (see Fig. 1) at the prime focus, and in the focal plane, of the telescope. Each beam had two channels, one left-circularly polarized, the other right-circularly polarized. In principle, this provided us with two independent views of the same patch of sky. However, in general, we averaged the channel outputs together during the reduction process to raise the signal-to-noise ratio. The two channels also provided useful redundancy in the event that one receiver channel malfunctioned.

We measured the beamwidths on the sky (full width at half maximum, FWHM) to be $4.2' \pm 0.1$. The receiver was rotated to an angle of 19.1° as shown in Fig. 1. In this configuration, the tracks of the beams on the sky formed seven parallel paths that were very close to being equally spaced at approximately one FWHM beamwidth.

As well as the PMN 4850 MHz surveys, we also made concurrent surveys at a frequency of 843 MHz using a separate, off-axis, single-beam receiver. The primary reason for these "serendipity" surveys was to provide low spatial frequency information for data taken using the University of Sydney's Molonglo Observatory Synthesis Telescope (MOST) instrument. In what follows we shall not discuss the 843 MHz data further. It is not intended to produce a full set of sky maps at this time but to use the data simply to assist in the small-area map-making of the MOST synthesis telescope.

2.2 Data-acquisition

We took data for the PMN Surveys using an analog-to-digital (A/D) converter that had a dynamic range of about 4000:1. Objects stronger than about 40 Jy were saturated in our survey, but the quantization effect on weak sources was smaller than the noise.

Although the receiver channels had low noise temperatures, the scans were still affected by low frequency variations due to atmospheric effects. This noise typically has a "$1/f$" character such that the noise amplitude increases when sampled on longer time scales (see, for example, Condon *et al.* 1989). To reduce the effects of this sky noise on our data, it was necessary to scan the telescope at the maximum possible rates. We calculated that the faster the telescope was scanned, the *better* (lower) would be the flux limit of the final surveys.

TABLE 1. Survey parameters.

Survey Name	Declination Range (deg)	Area (sr)	Track	Minimum time to survey (days)
Southern	-87.5 to -37	2.50	Meridian	10
Zenith	-37 to -29	0.74	Off-meridian	3
Tropical	-29 to -9.5	2.01	Meridian	6
Equatorial	-9.5 to +10	2.13	Meridian	8

All survey scans were made close to the maximum rate of 12 degs/min to maximize sensitivity in the presence of the $1/f$ noise from the atmosphere and to minimize the total observing time required.

3. OBSERVATIONS

The observations for the PMN Surveys took place during two sessions. The first session, called the "June session" in what follows, ran from 1990 May 29 to July 2. The second session, called the "November session," ran from 1990 October 31 to November 25. Survey observations took place 24 hours a day unless calibration or extenuating circumstances, such as mechanical failure or weather conditions, caused a shutdown of the telescope.

3.1 The Surveys and Scheduling

We divided the sky into several survey bands for ease of observation. We identify them in what follows by the names listed in Table 1.

The surveys described as having a "meridian" track in Table 1 were made by scanning the telescope alternately up and down the meridian ($HA=0^h$). As the sky moved past the telescope at the sidereal rate, data from different right ascensions was collected. It was not possible to scan fast enough to keep up with the motion of the sky. Therefore these surveys extended over several days.

Each scan track was 28′ wide on the sky, close to seven times the half-power beamwidth of 4.2′. At the typical scan rates used (about 11 degs/min), our sampling rate corresponded to a sample size of about 53″ on the sky.

The Southern, the Tropical, and the Equatorial Surveys all used the same basic observing technique described in more detail below. We were constrained to observe further than 3° from the zenith (to permit deceleration of the dish before encountering the zenith limit) and further than 2° from the south celestial pole. The Zenith Survey required a different approach because it was not possible to drive the telescope through the zenith nor rotate the receiver package. The Equatorial and Zenith Surveys will be described in more detail in later papers.

3.2 The Southern Survey

The Southern Survey was the largest section observed. It extended from $-87.5°$ to $-37.0°$ declination and over all right ascensions, an area of 2.50 sr. Scans were made by

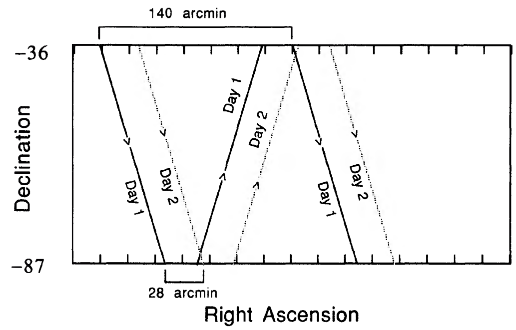

FIG. 2. A scan from the Southern Survey (solid lines) and the adjacent scan on the next day (dashed lines). Only the track of the central, on-axis beam is shown. The area of sky between the two tracks on Day 1 and Day 2 was covered by the six off-axis beams. The starting positions of the scans on successive days are separated by 28 arcmin, while the difference between the starting positions of two similarly-moving scans on the *same* day is 140 arcmin.

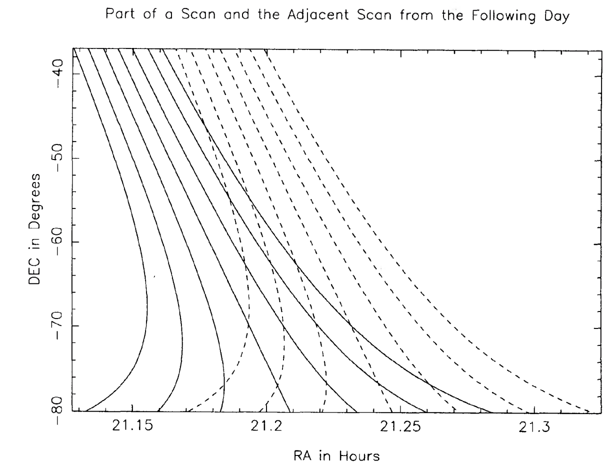

FIG. 3. The track of all seven beams of the 4850 MHz receiver from a Southern Survey scan (solid lines) and the adjacent scan for the next day (dashed lines). The beams "flare out" in right ascension as they approach the pole, but remain a constant 4′ apart on the sky. Notice also that the beams from the two adjacent days overlap as the scans approach the pole, increasing the signal-to-noise ratio at low declinations.

moving the telescope in zenith angle alternately north and south along the meridian (HA=0^h, azimuth=180°) at a rate of 11.1 degs/min.

To see how the sky was covered, refer to Fig. 2 that shows the track of the central beam (only) on the sky during two successive days. On any particular day, we scanned tracks on the sky spaced 140′ apart. The next day, our scans were displaced 28′ later than the scans done on the previous day. After 5 days, we had covered all right ascensions twice, once in a south-moving direction and once with the accompanying north-moving scans.

The sets of scans referred to in the previous paragraph, we called the "Regular" scans. However, to obtain adequate (Nyquist) sampling of the sky, a second set of "Nyquist" scans were made displaced from the Regular scans by approximately 0.5 FWHM beamwidths (2′). The set of Nyquist scans required an additional 5 days of observing. In all, we covered the sky four times: north-moving Regular scans, north-moving Nyquist scans, south-moving Regular scans and south-moving Nyquist scans.

The solid lines in Fig. 3 represent the tracks of the 7 beams of a Regular scan on an RA-Dec plot. The beams within a scan "flare out" in RA as we approach the pole but remain a constant 4′ apart on the sky. The dashed lines show the adjacent Regular scan from the next day. Note that the scans overlap as they approach the pole. When a scan reaches −64° declination, we have effectively doubled the coverage of the sky as compared to the northern end of the scan. This implies that the signal-to-noise ratio for the data will improve as we move southward in declination.

3.3 *The Tropical Survey*

For the Tropical Survey, the telescope was moved onto the northern meridian (HA=0^h, azimuth=0°). This effectively rotated the receiver by 180° relative to the equatorial coordinate system. In all other respects the scan patterns for this survey were essentially identical with those for the Southern Survey.

This survey extended from −29.0° to −9.5° declination over all right ascension, an area of 2.01 sr. The telescope scanned north and south at a rate of 11.3 deg/min between −30.0° and −8.5° declination for both the Regular and the Nyquist scans.

3.4 *Weather and Data Quality*

Scans done during periods of poor weather were checked for quality and, if necessary, reobserved during good weather. Some areas of the survey were contaminated by Solar radiation reflected from the telescope's focal cabin support legs (Hunt & Wright 1992). An area from declination −55° to −66° and RA 4.5^h to 6.0^h (coordinates in J2000) strongly affected by Solar radiation in June was reobserved in November and the new data used to replace the contaminated area. Other areas were less strongly affected and our reduction method removed the contamination from the data. Sources lying near these weakly affected areas are flagged in our final source lists (see Sec. 8).

4. CALIBRATION

The PMN Surveys required calibration for the pointing of the telescope, for the relative gains of the beams as a function of zenith angle, for the positions of the offset beams relative to the central feed, and for the absolute flux scale. Each of these calibrations required an intensive set of observations at the start of the survey. We also checked the calibrations occasionally throughout the survey to verify that none of the parameters had changed.

4.1 *Pointing Calibration*

For the PMN Surveys, more than 20 sources with accurately known positions were observed all over the sky before data acquisition began, in both the June and November sessions. These data were used to determine the pointing errors of the telescope.

As part of producing a final source list, previously known, strong sources with accurate positions from the PKSCAT90 database (Wright & Otrupcek 1990) were used to remove small, residual pointing errors caused by such effects as differential solar heating and gravitational deformation of the telescope.

4.2 Gain vs Zenith Angle Calibration

To calibrate the variation of telescope gain with zenith angle, we produced zenith-angle gain curves for each receiver channel. To do this we observed the strong radio sources PKSB 0521−365 and PKSB 1921−293 using all 14 receiver channels over the total range of zenith angles covered in the surveys. We determined that the flux errors introduced from uncertainties in these gain curves are approximately 1.6%.

4.3 Absolute Gain Calibration

A preliminary calibration of our data was made using a noise-calibration source for each channel. These noise sources were turned on and then off at the start of a scan and were calibrated by reference to the strong source PKSB 0915−118 (Hydra A) before observing began.

During the final stages of producing the source lists, we compared the PMN Fixed-Width flux densities (see Sec. *5.2*) for 23 strong point sources, with well-established spectra to the flux densities listed in the Kuhr *et al.* (1981) catalog. We find no significant systematic difference between the two sets of data. Flux densities in our published source lists therefore should be consistent with the Baars *et al.* (1977) flux scale, upon which the Kuhr *et al.* data list was based, and thus also with the northern surveys of Condon *et al.*

4.4 Orientation of the Beams on the Sky

Only the position of the central feed of the 7-beam receiver was recorded in our data files. Therefore, we needed to establish the orientation of the receiver and the angular distances from the central feed to the other six feeds, so as to reconstruct the other beams' positions on the sky. We measured these offsets by observing a strong point source with each of the 7 beams in rapid succession and noting the relative positions.

We made these measurements for both the June and November sessions. Our measurement of the average angular distance between the central feed and the other feeds of the 7-beam receiver was 12.1′±0.1. The orientation angle was the same for both the June and November sessions. We measured this angle to be 19.6°±0.3 (see Fig. 1), which is only 0.5° from the ideal orientation of 19.1°, a negligible amount. The overall uncertainty in the position of any offset beam was about 6″.

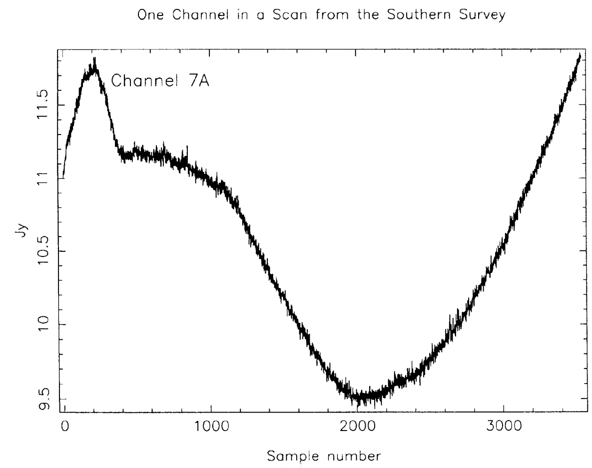

FIG. 4. The entire length of a scan from the Southern Survey for a single receiver channel of the 4850 MHz receiver. The shape of the curve comes from the varying amount of spillover of ground radiation as the dish moves from the zenith to the horizon. This gross shape was highly repeatable from scan to scan. The samples along the abscissa are 80 ms long.

5. DATA REDUCTION

The principal goal of the PMN project was to produce a point source catalog. This section describes the procedures followed during the data reduction.

The method used by Gregory & Condon (1991) relied on maps made by Condon *et al.* (1989) who convolved the scan data into a set of sky images. The maps were then used to obtain a source list using the DAOPHOT (Stetson 1987) finding routine. We decided that a better approach would be to make the point source catalog directly from the calibrated, but unconvolved, survey data. This follows since convolution in the presence of noise implies a loss of information if the Fourier transform of the convolving function has zeros (as was the case for Condon's sinc*Gaussian convolving function). Furthermore, Gregory and Condon's method produces a loss of spatial resolution in the convolved data. We choose to use the better procedure of fitting a profile matched to the beam on the raw data.

5.1 Stage 1: Processing of the Individual Scans

The first step in reducing the data was to convert the individual scan samples to mJy. This was done by dividing the size of all the samples in an individual scan by the average of the size of the noise-calibration measurements at the beginning and end of the scan. Then the sample values were multiplied by the absolute size of the relevant noise calibration for each channel measured using the source Hydra A (see Sec. *4.3*).

Secondly, we removed a gross or "canonical" baseline from each scan that depended only on zenith angle. Figure 4 shows an entire scan from the Southern Survey for one 4850 MHz receiver channel with the data converted to Jy. The shape of the curve largely results from the varying

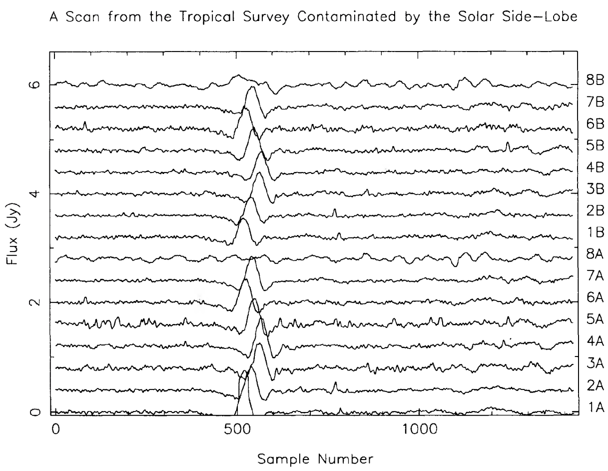

FIG. 5. Data from all receiver channels after removal of the "canonical" and median filter baselines. The vertical scale is in Jy but with an arbitrary zero point for each channel. Channels labeled 1A–7A and 1B–7B are from the 4850 MHz receiver: channels 8A and 8B are from the 843 MHz receiver. The large structure in the data near sample 500 is caused by the solar interference described in the text. The samples along the abscissa are 80 ms long.

amount of contamination from ground radiation as the dish moves between the zenith and the horizon.

Thirdly, the zenith-angle gain curves described in Sec. *4.2* were applied to the data on a beam-by-beam basis. That is, each sample value was divided by the zenith-angle gain derived from the appropriate curve and for the appropriate zenith angle.

Fourthly, we removed the gross effects of the solar side-lobe contamination from the scan data. Figure 5 displays the data from all receiver channels for a single contaminated scan. Channels marked 1–7 A and B contain data from the 4850 MHz receiver while channels 8A and 8B contain the data from the 843 MHz receiver.

The broad structure in the data near sample number 500 is the solar side-lobe contamination described earlier. We searched for such features in our data using a computer subroutine that looked for strong emission much broader than a telescope beamwidth. When a broad feature was found, a check was made against another subroutine that predicted where the side-lobes should be on the sky as a function of time and the Sun and dish's positions. If a broad feature was detected within 3° of the predicted position, the data within 1.0° of the feature center was "blanked" (i.e., flagged and removed from consideration). The only real astronomical objects that caused a solar side-lobe-like structure were the Galactic plane, the Large Magellanic Cloud (LMC), and an occasional bright extended galaxy. Our method permitted us to retain data on these real objects since they did not fall within 3° of the predicted position of the solar side-lobes.

Fifthly, we removed the effects of short-term, "spiked" interference in our data. The signature of interference could be recognized since it occurred in all receiver channels *centered on the same time sample*. On the other hand, real features in the sky occurred at different times in the various channels, since the beams were displaced relative to each other on the sky. We checked for interference by (temporarily) removing a simple, smoothed baseline from the data and looked to see if, at the same time, data in more than eight channels were above a limit of 70 mJy. If this criterion was met, we blanked these samples in all beams as interference. The interference filter was not applied when within 8° of the Galactic plane nor near certain large structures, such as Centaurus A and the LMC. These structures had high background levels that could cause the interference filter to wrongly blank much of the data in those regions.

Sixthly, we averaged the outputs of the left and right circularly polarized channels from each beam. This produced a useful increase in the signal-to-noise ratio for a given beam. In a few cases, the output from a given channel was obviously bad. In this case, we simply used the output from the other channel. Of course, averaging the two polarizations destroys any information on circularly polarized sources. However, since all the raw data from the survey has been preserved, a search for circularly polarized sources may be carried out later.

Seventhly, we removed the residual baseline (remaining after subtracting the canonical baseline) from each averaged scan using a median filter. Our choice of a median filter was made after making several tests on different sorts of filters. Using a median filter caused a downward bias to the flux density of sources. These "bias corrections" to the source flux densities are discussed in Sec. 6.

To reduce the chance that a source would seriously affect the median baseline, we required the width of the filter to be at least ten times the telescope's beamwidth. We experimented with increasing the width of the filter from this minimum until the rms noise on a channel started to rise. In this way, we could reduce the effect of a source on the filter without increasing the noise substantially. Our final choice was to use a median filter of width 65 samples, corresponding to about 57′ on the sky.

Eighthly, we blanked individual samples within a scan that were anomalously higher or lower than their neighbors so that they would not be mistaken as real features at a later stage in the reduction. A "spike" filter was applied to the data by looking at a point and its nearest neighbors within a beam. If a point differed by more than 100 mJy from the average of its neighbors and the difference divided by the average was >0.45, we blanked the point as anomalous. In addition, any point that was below -120 mJy was blanked as a "hole."

Ninthly, we corrected the declinations of the data samples in each scan for the effects of telescope "lag." We corrected for this by measuring the positions of a few bright sources found in the north-moving scans and comparing them to positions of the same sources found in the south-moving scans. The differences in positions were consistent and equal to twice the lag distance. We measured the lag for each survey separately. The recorded positions of a sample within a scan were corrected for this bias, which was close to 20″.

Tenthly, the final part of the first stage of the data processing placed the data on a grid having right ascension and declination (apparent coordinates) as the axes. We set the spacing between grid points to 1′. We chose this spacing because it is approximately the interval between the samples in Dec and about half the interval between samples in RA. A finer grid spacing would not have increased the positional information significantly and would have consumed much more computer time. A coarser grid spacing would have under sampled the data and would have introduced an unacceptable loss of positional information.

Each scan sample was "placed" on the grid point nearest to the actual, measured right ascension and declination of that sample. Blanked samples were ignored. The total flux on a grid point was averaged using the number of samples placed on each point. Because of our chosen grid resolution, some grid points were devoid of data. The grid of fluxes and the grid of counts were written to files for further processing.

5.2 Stage 2: Source Finding and Fitting—Pass 1

The first stage of processing calibrated, edited, and gridded the data. We then proceeded to search for sources on the grid and derive their positions, widths, and flux densities.

The search for a source started by looking at each point on the grid in turn and checking to see if it was a local maximum. If a grid point with a higher flux existed within rectangle $7 \cdot \sec(\delta)$ points wide in right ascension, and 7 points wide in declination (roughly $2 \cdot \sec(\delta) \times 2$ FWHM beamwidths) centered on the point under consideration, the central grid point was ignored and the search continued to the next point. If the central point had the highest flux in the search area, we called it a local maximum. The computer then attempted to fit a source to those grid points containing data in the $7 \cdot \sec(\delta) \times 7$ rectangle centered on this local maximum. A small proportion of sources extended appreciably beyond a rectangle of this size, but a fit that ignores the outer fringes of a source is sufficient to determine the size and shape of all but the most extended objects.

For every local maximum found on the grid, we first fitted a two-dimensional Gaussian having a fixed beamwidth (FWHM) of 4.2′. The Parkes telescope beam for the 4850 MHz surveys was measured to be very closely Gaussian and to have very low sidelobes. Because of this, we decided to fit sources using a simple Gaussian function rather than attempting to develop a more complex point-spread function as used by Gregory & Condon (1991). This first fit will be referred to as the "Fixed-Width fit" in what follows.

In this paper, we use the term flux density instead of peak brightness. This follows since the flux density (measured in mJy) and peak brightness (measured in mJy/beam) have the same numerical value for point sources. When we attempt to measure extension (see below), we use peak flux density to mean the peak of the brightness distribution. The integrated flux (i.e., flux density) can be obtained from the widths of the Gaussian fit and the peak flux density.

In the Fixed-Width fit, the flux density and position (right ascension and declination) of the Gaussian were free parameters. If the value determined for the flux density was $\geqslant$25 mJy and the fitted position was within 3′ of its local maximum point, we made a second fit to the data. If the fitted source was too weak or too far away from its local maximum, the fitted parameters were logged and we continued to the next grid point. (The 25 mJy limit was reduced to 15 mJy close to the South Pole where the overlapping scans and lower grid noise made this meaningful. However, for convenience in what follows, we shall still refer to this as the "25 mJy" criterion.)

It should be noted that the flux density from this Fixed-Width fit will overestimate the peak flux of a slightly extended source (and, conversely, underestimate the peak flux if the source appears narrower than the beam because of noise). On the other hand, our determined flux density will more closely approximate the integrated flux in both cases.

The second Gaussian fit allowed us to detect sources that were extended in either the right ascension or declination direction. We will refer to this as the "RA–Dec fit." The idea here is that a genuine astronomical source will have measured widths at least as large as the beam shape. However, a false source—caused, for example, by a noise spike, interference, or a receiver channel that went high for a short time—would have a narrow width in at least one direction (usually RA). The elimination of these abnormally shaped sources is discussed below.

A third, and final, fit was made to sources having flux densities $\geqslant$100 mJy and positions within 3′ of the local maximum based on the Fixed-Width fit. The purpose of this third fit was to detect and measure genuinely extended astronomical objects. We fitted a Gaussian having peak flux density, position, semi-major axis, semi-minor axis, and position angle as free parameters. We call this the "General" fit. However, because of the number of degrees of freedom permitted, it was only meaningful to try a General fit for the stronger sources.

The data from all three fits were recorded to a logging file for later use. A file was also kept of local maxima that failed the "flux density $\geqslant$25 mJy" and "position within 3′" criteria. See below for details on the use of these files for the second pass of source fitting.

5.3 Stage 3: Evaluation of Sources Found in Pass 1

The first pass at source fitting resulted in some objects that we regarded as "good" sources, some that were "questionable," and some we regarded as "bad" (based on their measured widths, for example).

We dubbed as "bad" those sources whose Fixed-Width flux density was less than 25 mJy, those which had a Fixed-Width fit position more than 3′ from the local maximum, or those which had inconsistent RA–Dec fit widths. Since our beam size was 4.2′, we expected the fitted widths to be at least this size. Figure 6 shows where a source's widths

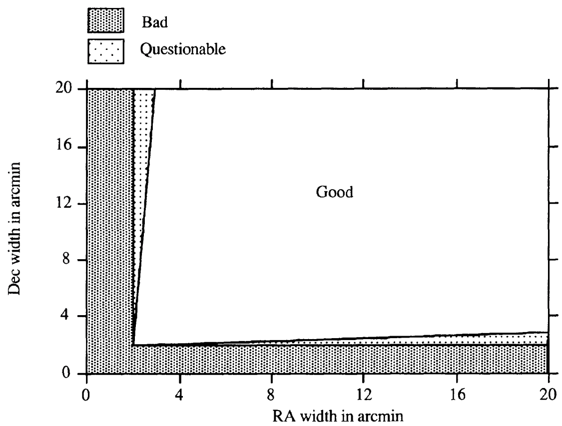

FIG. 6. The ranges in which the measured widths in right ascension and declination of a source must lie to be considered "good," "questionable," or "bad" on the basis of the "RA–DEC" fit, as described in the text.

had to lie to be considered in each category. In addition, we regarded as "questionable" any source that had its RA–Dec fit position more than 3′ from the position of the local maximum.

It was probable that the presence of either a strong "bad" or "good" source masked weak, but genuine, sources in their immediate vicinity. Therefore, we removed the known "good" and "bad" objects and made a second pass to the fitting process.

5.4 Stage 4: Source Finding and Fitting—Pass 2

Before starting the second pass at searching the grid, we first removed the sources that were considered "good" from the first pass. To do this, we subtracted from the data on the grid appropriate Gaussian functions having the fitted flux densities, widths, and positions. The pixel corresponding to the local maximum associated with the source was also blanked, thus permitting us to find weak neighboring objects.

Secondly, we blanked the local maxima of the "questionable" sources. A local maximum may have been a noise spike on a real source that caused the fit to lie too far from the true peak of the source. This gave a real source a second chance to be found.

Thirdly, we removed Gaussian fits to the "bad" sources and blanked their local maxima. This removed the bad spots from the grid and, again, allowed us to find nearby sources.

Fourthly, we blanked the local maxima and the nearest points on the grid along the declination direction for objects whose Fixed-Width fit parameters failed the "$\geqslant$25 mJy" and "position within 3′" criteria. This allowed us to find sources that may have been missed because of a noise spike.

Finally, we re-searched the grid as described above using the same criteria as during the first pass.

5.5 Stage 5: Evaluation of Sources from Pass 2 and Preliminary Source List

The same criteria we described previously were applied to sources found in the second pass, except that sources we would previously have regarded as "questionable" were now regarded as "good." The "good" lists from the two passes were combined to form a preliminary source list. In addition, if two or more sources were found within 3′ of each other, we kept only the brightest of the sources.

Finally, we located sources stronger than 100 mJy in the preliminary source list and examined weaker objects within a radius of 11′ around them. Some such weak objects were likely to be artifacts of the strong source fitting process. We eliminated weak objects from our list based on a flux-ratio and resolution criterion. Specifically, if the flux ratio of the stronger to weaker source was R and the distance of the weak source from the strong source was less than a critical value D, the weak source was dropped from our preliminary list as a likely artifact. The distance D was related to a Rayleigh criterion for resolution and was given by

$$D=5.0+2.0\log_{10}(R)-0.2[\log_{10}(R)]^2 \text{ arcmin.} \quad (1)$$

This completed the compilation of the preliminary source list. Sources from each survey were held in separate lists, as were the objects found from the June and November observing sessions. The next stages of the reduction process were to combine the data taken during the June and November sessions, estimate biases and errors for objects in the preliminary list and set flux limits for the surveys.

5.6 Combining the June and November data

Originally, we had planned to omit the area of the June data contaminated by the solar radiation and replace the area with data taken in November. But the algorithm that removed the solar contamination from the June scans worked so well that we replaced only the small portion of the June data from declination $-55°$ to $-66°$ and RA 4.5^h to 6.0^h (coordinates in J2000) with November data. In the final source list, those sources found in June or November are flagged differently. We found no residual problems from the solar contamination in the Tropical Survey June data.

5.7 Limitations of our Reduction Process

It is important to realize that our reduction procedure was optimized for *point* sources; that is, objects whose angular extent was appreciably less than the FWHM of the telescope beam (4.2′). Very extended objects will undoubtedly have been missed by our reduction process, even if their integrated fluxes lie well above our limits. To find such objects, it will be necessary to study the raw, gridded data. Even then, the application of the median filter will have removed some low spatial frequencies from the source structure. Occasionally, a very extended object may be reported as a set of close point sources.

On the other hand, *mildly*-extended, weak objects will have a listed Fixed-Width flux density that approximates their integrated flux and be correctly included in our source lists. This follows from the nature of our Fixed-Width fitting process (see Sec. *5.2*). Strong (> 100 mJy) extended sources will be obvious from the General fit.

Finally, very strong sources (typically with peak flux densities greater than about 30 Jy) will have been affected by saturation of the A/D unit and their measured flux densities will be unreliable. In addition, very strong *extended* sources may have been omitted from our source list altogether by the application of the interference filter.

6. CORRECTIONS AND ERROR ESTIMATES

The preliminary source lists described above contained objects with measured flux densities greater than 25 mJy (or lower near the South Pole, as mentioned above). Undoubtedly, many objects whose true flux densities were greater than 25 mJy will have been missed from this list because of the effects of noise. For a similar reason, many objects with true flux densities much less than 25 mJy will appear in our list. In addition, our reduction process imposed several biases on the source flux densities. This section details how we determined the actual noise levels and discusses the corrections to the flux densities of sources.

6.1 Artificial Source Injection Tests on a Noisy Grid

Our most powerful tool for determining many statistics for the PMN Surveys was a set of artificial source injection tests. These "Monte Carlo" tests were made by adding artificial point sources at random positions into the left-circularly polarized real scan data and adding *negative* artificial sources of equal strength to the right-circularly polarized data at the same positions. We then processed the data using almost exactly the same techniques described previously. The exception was that, instead of averaging the two polarization channels from a beam, we subtracted them and divided by two.

The effect of this was to remove all real sources from the data (with the possible exception of a few circularly-polarized sources) leaving us with just noise and the injected sources. Provided that the noise from the receiver channels with left-circular polarization was uncorrelated with the noise from the corresponding right-circular polarization channels, the resulting noise statistics would be the same whether we added the channels or subtracted them. We verified that this was indeed the case.

This process left a grid containing our injected, artificial sources with known true intensities, with known true widths, with known true positions and having the same noise statistics as for the real data. In essence, we had created a synthetic universe. Since the data from each scan with injected sources was processed identically to the scans used to determine real sources, we preserved all the biases caused by the reduction method. Only effects due to gain and some effects of ground radiation that occurred in the real data could not be mimicked exactly in the synthetic data.

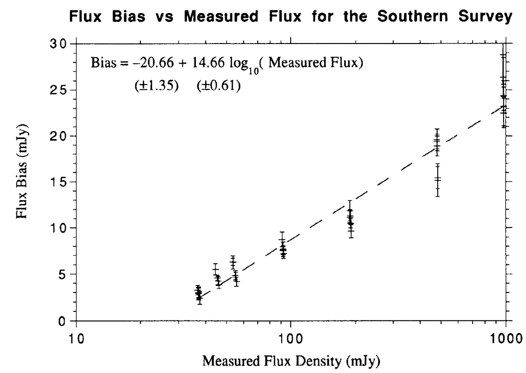

FIG. 7. Plot of the difference between injected and measured flux density against measured flux density for objects used in the Monte Carlo injection simulations. The data comes from various declination ranges. However, a single curve fits the data to sufficient accuracy. This fit was used for applying a correction bias to the flux density of the real sources.

6.2 Systematic Corrections to the Source Flux Densities

The flux densities of sources appearing in our source lists are affected by small, but significant biases. These arise from such effects as the application of the median filter to a scan, gridding the data and by the process of fitting a Gaussian source in the presence of noise. For a more detailed description of some of these effects see Condon *et al.* (1989).

To assess the importance and sizes of these biases, we used the artificial source injection tests. For a one hour-wide section of the Southern and Tropical Surveys, we injected 1000 sources with identical flux densities of 40 mJy. We repeated this for source strengths of 1000, 500, 200, 100, 60, and 50 mJy. By comparing the reported flux densities to those known to have been injected, we determined the biases resulting from our reduction package. We divided the survey into several declination bands, but found one function fitted all bands well. We fitted the data to a function of the form $\mathrm{BIAS}=A+B.\log_{10}(S)$, where S is the measured flux density and the flux bias is defined as (*True (injected) flux density* $-S$). We estimated the uncertainty in the bias correction caused by the effects of faint confusing sources to be less than 1% of the bias, which is negligible for our purposes.

Figure 7 shows the results of these tests for the concatenation of all declination bands of the Southern Survey. The ordinate is the flux bias and the abscissa is the logarithm (base 10) of the measured flux density after processing. The data is well fitted for all declinations by:

$$\mathrm{BIAS}=-20.66+14.66.\log_{10}(S), \tag{2}$$

where BIAS and S are in mJy. The standard errors in the two fitted parameters were 1.35 and 0.61, respectively. For the Tropical Survey, the fitted parameters were essentially the same. Therefore, the above formula was used to apply corrections to the flux densities of all the listed sources.

6.3 Positional Accuracy

We examined the positional accuracy of the sources appearing in our source lists using two methods. First, we compared the positions of the injected sources to those fitted by the reduction process. In general the standard errors (s.e.) in right ascension and declination are well represented by a constant term added in quadrature with a term inversely proportional to the flux density of the source.

Our second method compared 265 known, strong, PKSCAT90 sources having accurate (s.e. $<2''$) positions (Wright & Otrupcek 1990) to their PMN counterparts. On the basis of this comparison, we removed small, systematic, residual pointing errors by adjusting the positions of all the PMN sources. Following this operation, the remaining, random standard errors were found to be consistent with the formulas:

$$(\text{s.e. in RA})^2=(1300/S)^2+(6)^2, \tag{3}$$

$$(\text{s.e. in DEC})^2=(1100/S)^2+(4)^2, \tag{4}$$

where the standard errors are in arcseconds and S is in mJy.

In principle, the position errors should be somewhat less at the more southerly declinations where the flux errors are lower. However, in practice, the above equations adequately represent the positional errors over all declinations.

6.4 Flux Density Errors

The standard error on the flux density of any source is a combination of the error on the fitted flux density of a source resulting from random noise on the gridded data, the errors introduced by gain fluctuations, the background confusion of faint sources, and the errors introduced by uncertainties in correcting the source flux densities for the biases mentioned above. We have adopted a value of 2 mJy for the rms confusion of the Parkes telescope at 4850 MHz (Wright 1992). Using the values we determined from the artificial source injection tests, we estimated the standard error on the flux density of a source (in mJy) to be

$$\text{s.e.}^2=\text{EF}^2+(2)^2+(0.016.S)^2+(\text{EB})^2. \tag{5}$$

In the above equation, EF is the flux fitting error, the factor of 2 is the error from confusion, the factor of 0.016 is the gain error discussed previously and EB is an error resulting from uncertainties in the flux bias correction. Typically, EB was 1 mJy or 0.6 $\log_{10}(S)$ mJy, whichever was greater. The flux fitting error, EF, was determined from our Monte Carlo simulations in each declination band and can be approximated for the Southern Survey by

$$\text{EF}^2=(11.8+0.085\delta)^2+(0.050.S)^2, \tag{6}$$

where S is in mJy and δ is the declination in degrees.

The total standard error on the flux density for the Southern Survey thus can be obtained with sufficient accuracy from:

$$\text{s.e.}^2=(12.3+0.085\delta)^2 + (0.052.S)^2\ (\text{mJy}^2)\quad (\text{Southern Survey}). \tag{7}$$

The corresponding formula for the Tropical Survey is

$$\text{s.e.}^2=(10.5)^2 + (0.052.S)^2\ (\text{mJy}^2)\quad (\text{Tropical Survey}). \tag{8}$$

These standard errors are listed alongside the source flux densities in our final source lists. A standard error of >99 mJy is listed as "99" mJy because of space limitations: exact values may be calculated from the above equation in such cases.

7. RELIABILITY, COMPLETENESS AND FLUX LIMITS

Large area radio catalogs are characterized by three important parameters: reliability, completeness, and the flux limit. Reliability measures the probability that a source appearing in the catalog is "real." Completeness measures the probability that a genuine source, having a certain strength, will appear in the catalog. The flux limit determines how many sources, both reliable and unreliable, will appear in a catalog. In practice, reliability and completeness are notoriously difficult quantities to estimate. Furthermore, they have been defined in different ways for previous catalogs.

7.1 Determining the Reliability

What do we mean by reliability? This concept is related to defining what we mean by "real."

If a source is measured to be 52 mJy, but is later determined to have a true flux density of 48 mJy, do we consider the source real? If the catalog flux limit were set at 50 mJy, some definitions of reliability would consider this source unreliable since its true flux density lies below the catalog flux limit. In this paper, we choose to define a source as "real" if the "true flux density" of a source lies close to the measured flux density. From the Monte Carlo injection tests, we find that the average difference between true and measured flux densities is a small fraction of the cataloged flux density.

Using this definition of "real," we define the reliability as follows. In a given catalog, let there be N_a sources with measured flux densities greater than some value S_0. Let N_b of these sources be real with true flux density close to the measured flux density. We define the integral reliability at flux density S_0 as the ratio N_b/N_a.

Reliability as defined above refers to the cumulative sources in a catalog. In this paper, we prefer to use the more useful concept of *differential* reliability defined over a given, small flux range.

Normally, one estimates the reliability of a survey by comparing it with a small area survey having a lower flux limit or by remeasuring a large number of objects appearing in the catalog. For the PMN Surveys, however, we decided that a more accurate estimate of this quantity could be obtained from the artificial source injection tests.

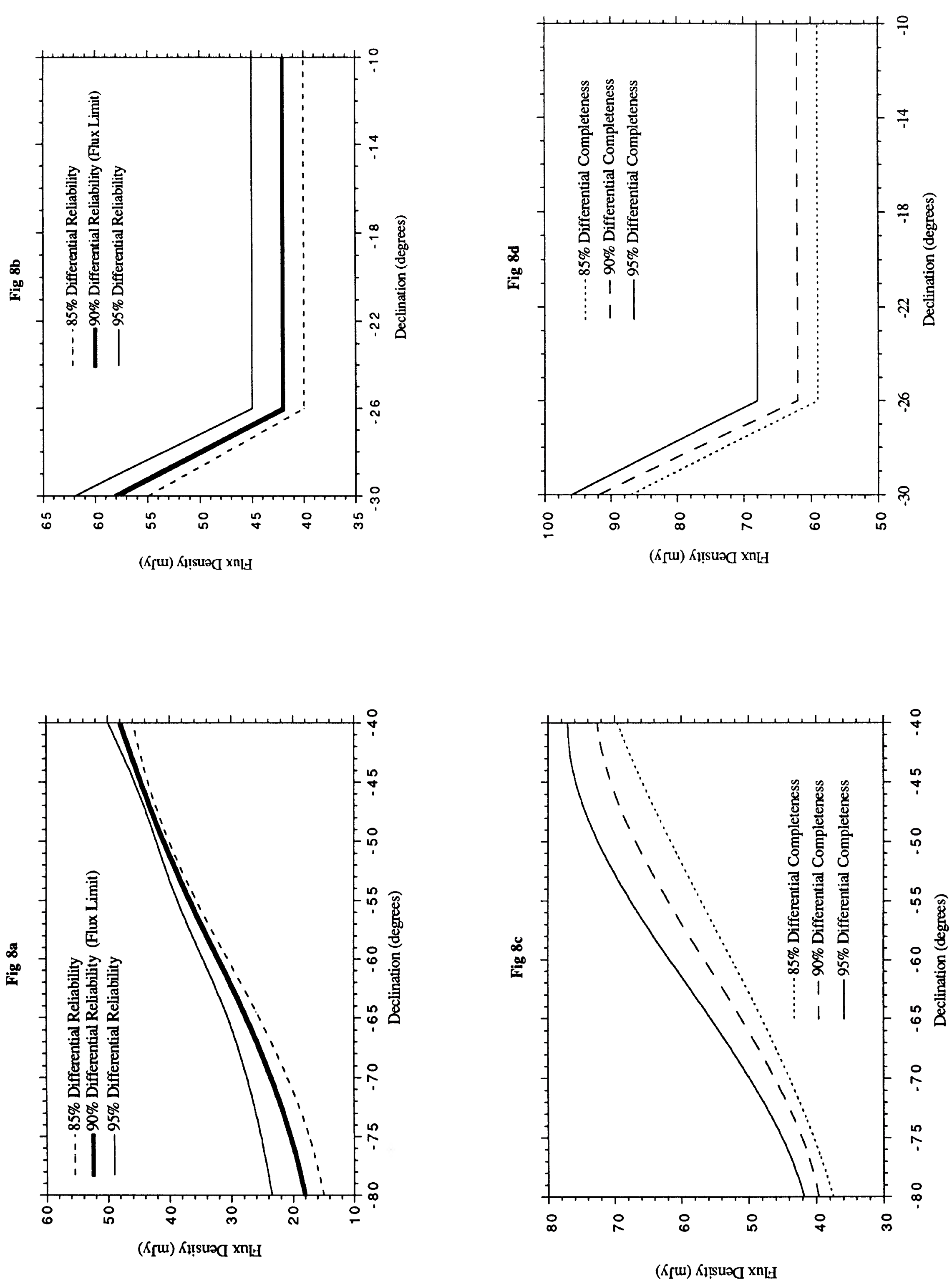

FIG. 8. (a)–(d) Plot of flux density vs declination for differential reliabilities of 85%, 90%, and 95% as explained in the text for the Southern Survey (a) and for the Tropical Survey (b). (c) (Southern) and (d) (Tropical) show similar plots but for differential completenesses of 85%, 90%, and 95%.

We estimated the differential reliability of our surveys, in a given flux range and within a given declination band, by one-to-one matching of the artificial sources our reduction process finds to the objects known to have been injected.

For these tests, we created a synthetic universe of sources as described in Sec. *6.1* and based on the source counts published by Bennett *et al.* (1985). Sources were injected at random positions and in appropriate numbers with flux densities ranging from 5 to 5000 mJy. In addition, the density of injected sources was chosen to be similar to the Northern Hemisphere source density. The use of the real source counts appropriately modeled the possibility of a weak source being masked by a strong source.

Figures 8(a) and 8(b) show plots of flux density versus declination for differential reliability estimates of 85%, 90%, and 95% for the Southern and Tropical Surveys.

7.2 Determining the Completeness

In this paper, we define completeness as follows. Let there be N_c sources in the area of sky surveyed with true flux densities greater than some value S_0. Let N_d of these sources have a measured flux density both close to the true flux density (real as defined above) and greater than the catalog flux limit. Integral completeness is then defined as N_d/N_c. In this paper, we use the *differential* completeness defined as above except for sources in a small flux range.

The same Monte Carlo simulations used for the reliability estimates were used to make estimates of the differential completeness. Figures 8(c) and 8(d) show plots of the flux density versus declination for differential completeness estimates of 85%, 90%, and 95% for the Southern and Tropical Surveys.

7.3 Flux Limits for the Southern and Tropical Surveys

The flux limit for a survey can be defined in several different ways. Many previous surveys used a limit of five times the standard error on the flux of a typical source, the so-called "5-σ" limit. For Condon's survey, the 5-σ limit was based on the noise in his maps. For the PMN Surveys, we decided that it would be more meaningful and useful to define limits based on the differential reliabilities of our source lists. However, we also estimated values based on the noise and provide them for comparison.

Before proceeding further, however, it is reasonable to ask why such an apparently high level of significance as 5-σ is required. On the basis of Gaussian noise statistics, an object with a flux density five times greater than the noise should be reliable at a $>99.9\%$ level of significance. But this is not the case. First, the noise statistics are *not* Gaussian. Secondly, while the number of pure "noise bumps" appearing in the source list at the 5-σ level may indeed be very small, the number of objects that have a true flux density somewhat less than the limit and are elevated by noise to just above that limit, can be much higher. This is particularly true since the slope of the differential source counts predicts that the number of objects in any flux range

TABLE 2. Flux limit and 4.4-σ value for selected declinations.

	Declination (degrees)	Flux Limit (mJy) (90 % Reliability)	4.4 – σ Value (mJy)
Southern Survey	−80	20	24
	−70	24	28
	−60	32	32
	−50	40	35
	−40	48	39
Tropical Survey	−29	55	46
	−25	42	46
	−20	42	46
	−15	42	46
	−10	42	46

lying just *beneath* any given flux value is greater than the number of objects lying in a similar range just *above* that value.

In their classic paper, Murdoch *et al.* (1973) provided a detailed analysis of these points. They concluded that the 5-σ limit was highly appropriate for cases where the differential slope of the underlying source distribution was equal to -2.5 [where the slope is defined by $d\log(dN/dS)/d\log(S)$]. For the frequency and flux range of the PMN Surveys, however, the underlying distribution has a differential slope of close to -1.6 (derived from data in Bennett *et al.* 1985). We used the same analysis as Murdoch *et al.*, to show that a 4.4-σ limit provides the same reliability for a differential slope of -1.6 as does a 5-σ limit for sources with slope -2.5.

For the Southern and Tropical Surveys, we divided the objects into declination bands. We established a different flux limit for each band based on a 90% differential reliability in a 5 mJy wide bin. These limits were then fitted to simple functions of the form:

$$S_{\rm lim}=79.8+0.793\delta \text{ mJy}, \tag{9}$$

$$\text{or}=20 \text{ mJy} \quad \text{for} \quad \delta<-75^\circ \text{ (Southern Survey)}, \tag{10}$$

and

$$S_{\rm lim}=42 \text{ mJy (Tropical Survey},-26^\circ<\delta<-9.5^\circ), \tag{11}$$

$$S_{\rm lim}=-70.7-4.33\delta \text{ mJy (Tropical Survey},-29^\circ<\delta<-26^\circ), \tag{12}$$

where δ is in degrees. Since the scans became progressively more overlapped during the Southern Survey as we approached the Pole, the signal-to-noise ratio increased and therefore the flux limit decreased.

Table 2 shows the flux limits for the Southern and Tropical Surveys derived from the above equations for several typical declinations. The flux limits for the November data were essentially the same. This table also shows a 4.4-σ value based on the standard errors for the weakest sources found in each declination band. The ratio of our 90% differential reliability flux limit and this 4.4-σ value is not constant because the differential reliability estimates are more sensitive to problems with the baseline than are the errors on the flux from which the 4.4-σ values are calculated. We believe that the differential reliability limit is more appropriate for our surveys since it is obtained di-

TABLE 3. Sample source list.

Name	RA2000	Dec2000	Flux	SE	SI	D	X	G	Z	S	P	M
PMNJ0000-4618	00:00:01.6	-46:18:38	60	9		J						
PMNJ0000-4910	00:00:09.1	-49:10:59	59	9		J						
PMNJ0000-5207	00:00:09.7	-52:07:08	43	8		J						
PMNJ0000-6543	00:00:13.9	-65:43:13	30	7		J						
PMNJ0000-3822	00:00:16.5	-38:22:04	90	10		J						
PMNJ0000-8539	00:00:19.8	-85:39:46	98	7		J						
PMNJ0000-8248	00:00:24.1	-82:48:35	180	11	-0.9	J	X				P	M
PMNJ0000-4722	00:00:28.0	-47:22:05	133	11	0.0	J					P	
PMNJ0000-7142	00:00:30.8	-71:42:04	39	7		J						
PMNJ0000-6554	00:00:36.4	-65:54:10	51	7		J						
PMNJ0000-4958	00:00:37.1	-49:58:49	61	9		J						
PMNJ0000-8316	00:00:41.2	-83:16:33	24	5		J						
PMNJ0000-3923	00:00:46.8	-39:23:52	75	10	-0.8	J					P	
PMNJ0000-4517	00:00:48.4	-45:17:40	45	9		J						
PMNJ0000-6740	00:00:48.6	-67:40:37	27	7		J						
PMNJ0000-6230	00:00:50.0	-62:30:00	49	7		J						
PMNJ0000-6340	00:00:58.5	-63:40:57	69	8		J						M
PMNJ0000-6632	00:00:58.8	-66:32:52	79	8		J						
PMNJ0000-8341	00:00:59.9	-83:41:49	55	6		J						
PMNJ0001-7051	00:01:04.0	-70:51:29	76	7		J						
PMNJ0001-3703	00:01:04.9	-37:03:21	79	10		J						
PMNJ0001-7702	00:01:09.6	-77:02:34	52	6		J						
PMNJ0001-7511	00:01:10.7	-75:11:53	113	8		J	X					
PMNJ0001-6715	00:01:20.8	-67:15:46	80	8		J						
PMNJ0001-4630	00:01:22.3	-46:30:08	128	11	0.1	J					P	M
PMNJ0001-7609	00:01:24.7	-76:09:07	124	9	0.1	J					P	M
PMNJ0001-7546	00:01:28.4	-75:46:06	25	6		J						
PMNJ0001-8329	00:01:30.5	-83:29:15	27	5		J						
PMNJ0001-4513	00:01:44.0	-45:13:55	49	9		J						
PMNJ0001-3931	00:01:44.8	-39:31:01	95	10		J						
PMNJ0001-6849	00:01:46.0	-68:49:36	148	10	-1.1	J	X				P	
PMNJ0001-8458	00:01:54.3	-84:58:42	48	6		J						
PMNJ0002-8542	00:02:01.6	-85:42:45	34	5		J						
PMNJ0002-6122	00:02:18.6	-61:22:06	148	10	-1.3	J					P	M
PMNJ0002-5206	00:02:32.3	-52:06:51	47	8		J						
PMNJ0002-7757	00:02:38.6	-77:57:05	37	6		J						
PMNJ0002-5025	00:02:39.9	-50:25:08	94	9	-0.8	J					P	M
PMNJ0002-4305	00:02:41.8	-43:05:58	57	9		J						
PMNJ0002-5621	00:02:53.6	-56:21:07	401	22	-0.7	J					P	M
PMNJ0002-5948	00:02:56.2	-59:48:44	36	7		J						
PMNJ0002-4818	00:02:56.7	-48:18:01	46	9		J						
PMNJ0003-5529	00:03:07.4	-55:29:51	48	8		J						
PMNJ0003-7732	00:03:07.4	-77:32:02	25	6		J						
PMNJ0003-5444	00:03:10.7	-54:44:55	590	32	-0.3	J					P	M
PMNJ0003-5905	00:03:13.6	-59:05:39	159	11		J						M
PMNJ0003-8154	00:03:15.0	-81:54:37	23	5		J						
PMNJ0003-4517	00:03:15.9	-45:17:43	60	9		J						
PMNJ0003-6701	00:03:28.8	-67:01:53	56	7		J						M
PMNJ0003-6059	00:03:34.1	-60:59:38	34	7		J						
PMNJ0003-7702	00:03:50.1	-77:02:09	42	6		J						
PMNJ0003-4114	00:03:50.3	-41:14:59	72	10	-0.7	J					P	
PMNJ0003-5343	00:03:53.5	-53:43:43	58	8		J						
PMNJ0003-3827	00:03:55.6	-38:27:04	165	12	-0.8	J					P	M
PMNJ0004-4033	00:04:01.4	-40:33:10	74	10		J						
PMNJ0004-5112	00:04:05.0	-51:12:41	60	9		J						
PMNJ0004-4345	00:04:06.7	-43:45:17	223	14	-0.4	J					P	
PMNJ0004-4930	00:04:12.3	-49:30:25	47	8		J						
PMNJ0004-6413	00:04:13.7	-64:13:39	71	8		J						
PMNJ0004-5254	00:04:14.0	-52:54:39	316	18	-0.9	J					P	M
PMNJ0004-5546	00:04:19.3	-55:46:58	298	17	-0.6	J					P	M
PMNJ0004-5733	00:04:26.6	-57:33:01	39	8		J						
PMNJ0004-6102	00:04:27.1	-61:02:02	33	7		J						
PMNJ0004-4144	00:04:32.8	-41:44:03	120	11	-0.7	J					P	M
PMNJ0004-6656	00:04:35.5	-66:56:11	37	7		J						
PMNJ0004-4736	00:04:36.4	-47:36:10	708	38	0.2	J					P	
PMNJ0004-4824	00:04:38.8	-48:24:40	44	8		J						
PMNJ0004-6830	00:04:40.9	-68:30:03	26	7		J						
PMNJ0004-5122	00:04:57.2	-51:22:52	112	10		J						M
PMNJ0004-3713	00:04:58.8	-37:13:58	92	10		J						
PMNJ0005-5222	00:05:01.1	-52:22:30	49	8		J						
PMNJ0005-6804	00:05:01.4	-68:04:11	34	7		J						
PMNJ0005-5049	00:05:09.0	-50:49:23	90	9		J						
PMNJ0005-6649	00:05:17.5	-66:49:52	116	9		J						M
PMNJ0005-3920	00:05:19.8	-39:20:12	57	9		J						
PMNJ0005-6222	00:05:20.8	-62:22:07	139	10		J	X					
PMNJ0005-5542	00:05:24.3	-55:42:21	60	8		J						
PMNJ0005-5751	00:05:25.0	-57:51:48	198	13	-1.0	J					P	M
PMNJ0005-5428	00:05:36.3	-54:28:20	149	11	-1.3	J					P	M
PMNJ0005-8006	00:05:50.4	-80:06:25	65	6		J						
PMNJ0005-6255	00:05:51.2	-62:55:45	119	9	-0.9	J					P	M
PMNJ0005-6513	00:05:52.2	-65:13:40	66	8		J						
PMNJ0005-5822	00:05:55.2	-58:22:23	44	8		J						
PMNJ0005-5628	00:05:57.4	-56:28:36	677	36	-0.8	J					P	M
PMNJ0005-6451	00:05:57.5	-64:51:51	70	8		J						M
PMNJ0006-5001	00:06:00.3	-50:01:19	144	11	-0.6	J					P	
PMNJ0006-4234	00:06:01.2	-42:34:35	589	32	-0.9	J					P	M
PMNJ0006-6035	00:06:03.0	-60:35:43	98	9		J						
PMNJ0006-6854	00:06:07.2	-68:54:06	28	7		J						
PMNJ0006-5621	00:06:11.3	-56:21:11	41	8		J						
PMNJ0006-8305	00:06:15.6	-83:05:50	865	45	-0.4	J					P	M
PMNJ0006-7103	00:06:16.9	-71:03:12	25	6		J						
PMNJ0006-4245	00:06:20.8	-42:45:26	133	11	-0.6	J					P	
PMNJ0006-7312	00:06:21.5	-73:12:54	43	6		J						
PMNJ0006-8140	00:06:26.0	-81:40:31	35	6		J						
PMNJ0006-5216	00:06:33.9	-52:16:55	40	8		J						
PMNJ0006-6923	00:06:39.8	-69:23:02	36	7		J						
PMNJ0006-6909	00:06:40.9	-69:09:59	128	9	-0.8	J					P	M
PMNJ0006-7239	00:06:43.4	-72:39:21	31	6		J						
PMNJ0006-5259	00:06:50.5	-52:59:31	127	10	-1.0	J					P	
PMNJ0006-4620	00:06:52.1	-46:20:52	68	9		J						
PMNJ0006-7434	00:06:56.1	-74:34:05	41	6		J						
PMNJ0006-4022	00:06:58.1	-40:22:12	54	9		J						
PMNJ0006-4059	00:06:58.1	-40:59:59	53	9		J						
PMNJ0007-3934	00:07:02.5	-39:34:50	59	9		J						
PMNJ0007-5953	00:07:11.1	-59:53:33	120	10	-0.8	J					P	M
PMNJ0007-6741	00:07:12.5	-67:41:30	40	7		J						
PMNJ0007-6112	00:07:17.3	-61:12:54	224	14		J						
PMNJ0007-4023	00:07:17.9	-40:23:58	94	10		J						
PMNJ0007-7933	00:07:22.1	-79:33:17	25	6		J						
PMNJ0007-4313	00:07:23.6	-43:13:16	54	9		J						
PMNJ0007-4117	00:07:33.7	-41:17:22	53	9		J						
PMNJ0007-4548	00:07:46.4	-45:48:51	122	11		J						
PMNJ0007-8111	00:07:51.4	-81:11:25	49	6		J						
PMNJ0008-5243	00:08:03.7	-52:43:42	183	12		J						
PMNJ0008-3945	00:08:08.3	-39:45:18	322	19		J						
PMNJ0008-6247	00:08:10.7	-62:47:52	40	7		J						
PMNJ0008-5907	00:08:13.6	-59:07:47	173	12	-0.6	J					P	M
PMNJ0008-5009	00:08:30.1	-50:09:47	42	8		J						
PMNJ0008-5950	00:08:35.1	-59:50:34	40	7		J						
PMNJ0008-7511	00:08:36.3	-75:11:32	21	6		J						

rectly from Monte Carlo simulations of the reliability using the relevant noise statistics and underlying faint source distribution.

As a further test of the reliability of the weakest objects listed in our survey, we have compared the measured flux densities of artificial sources from the injection tests to the true (injected) flux densities of corresponding objects. If our flux limits were reliable, we should expect most of the objects to have a true flux density close to their measured flux density. On the other hand, if the reliability of the source list was low, then we should expect the true flux densities to be much smaller than their measured flux densities (see Murdoch *et al.*). We find that the standard deviations of the differences of the measured and true flux densities are typically less than 10 mJy, implying that the effects of noise are relatively small and confirming the high differential reliability for sources with flux densities near our stated limits.

Finally, we have compared sources in a region that was observed in both the June and the November sessions. This region contained about 400 objects and was free of solar interference in both sessions. The numbers and the flux density differences of the objects found in both sessions are consistent with the reliabilities, completenesses and flux standard errors quoted above.

8. SOURCE LISTS FOR THE SOUTHERN AND TROPICAL SURVEYS

The final source list for the Southern Survey contains 23 277 sources to the flux density limits given in Table 2. The Tropical Survey list contains 13 363 sources. Together, these surveys cover 4.51 sr of the southern sky between $-87.5°$ to $-37°$ and $-29°$ to $-9.5°$ declination (J2000) and across all right ascensions. In a few cases, the listed flux density of a source lies fractionally below the stated flux limit because of the 1 mJy precision of the listed flux densities. These lists will be available soon in both printed and machine-readable form.

Table 3 shows a sample page from the printed list. The PMN source names have been derived from their J2000 coordinates, in a similar manner to that used in the PKSCAT90 catalog (Wright & Otrupcek 1990) and following the IAU recommendations of Dickel *et al.* (1987). The flux density is listed with our estimate of the standard error on the flux density.

The columns in this Table are:

Name: The J2000-derived source name. The first three letters, PMN, denote the Parkes–MIT–NRAO survey, and the fourth letter denotes that the equinox and equator is J2000. The rest of the name is derived from the hours and minutes of the right ascension and the degrees and minutes of the declination (both J2000). For a few objects, the names (but not the sources) are duplicates: in such cases we have appended an "a" or "b" to the name.

RA2000: The J2000 right ascension as hh mm ss.s.

Dec2000: The J2000 declination as ±dd mm ss.

Flux: The 4850 MHz flux density in mJy derived from the Fixed-Width fit.

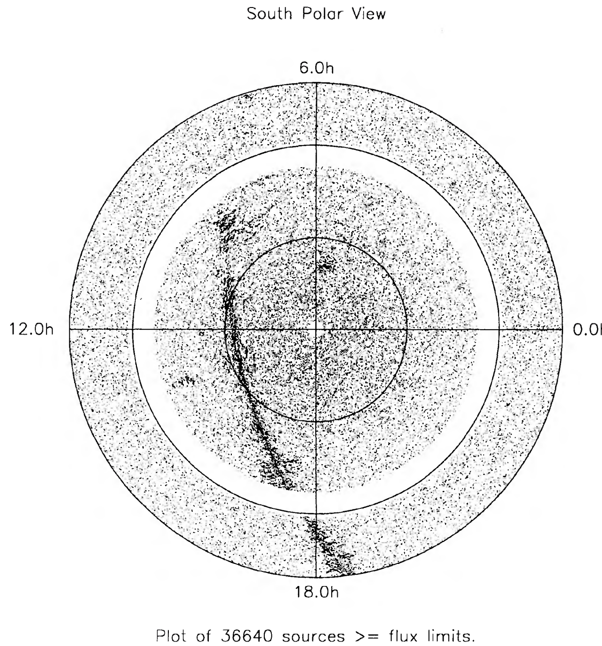

FIG. 9. View of all sources found in the Southern and Tropical Surveys above the quoted flux density limits. The plot is centered on the South Celestial Pole ($-90°$ declination), the inner rings mark declinations of $-60°$ and $-30°$, and and the outer ring is at $-9.5°$ declination. RA is labeled on the outer ring and increases counterclockwise. The 8° gap corresponds to the zone centered on the local zenith at Parkes ($-33°$ Dec), through which the telescope could not move. The dark band across the map is the Galactic plane. The LMC is near 5.5^h RA and $-69°$ Dec, and Centaurus A (Cen A) near 13^h RA and $-42°$ Dec.

s.e.: The estimated standard error on the listed flux density. A standard error >99 mJy is listed as 99 mJy because of space limitations: the accurate value can be obtained from Eqs. (7) and (8).

SI: The spectral index α computed between 2700 MHz from PKSCAT90 and the present flux densities at 4850 MHz. This index is defined by the equation $S \propto \nu^{\alpha}$.

The final columns denote various flags with the following meanings.

D: The session in which the source was observed. "J" indicates the June session and "N" the November session.

X: indicates that the source is probably extended.

G: indicates that the source lies within 10° of the Galactic plane.

Z: indicates a weaker source ($S<60$ mJy) that was observed within 6° of the Parkes telescope's zenith. Such objects may be affected by residual problems in baseline removal and the data may be of lower quality.

S: indicates that the source lay within 5° of solar contamination and the data listed may be of lower quality.

P: indicates that this source lies within 2′ of a source listed in the PKSCAT90 catalog and is probably the same object.

M: indicates that this source lies within 2′ of a source listed in the Molonglo 408 MHz catalog (Large *et al.* 1981) and is probably the same object.

Figure 9 shows a view centered on the south celestial pole of all the PMN sources found in the Southern and Tropical Surveys. The center point of the plot corresponds to declination −90°, the inner rings mark declinations of −60° and −30°, and outer circle of this plot corresponds to declination −9.5°. The RA is labeled and increases counterclockwise. The 8° gap corresponds to the zone centered on the local zenith at Parkes (−33° Dec), through which the telescope could not move. The dark band across the map is the Galactic plane. Note the Large Magellanic Cloud (LMC) that lies near 5.5^h RA and −69° Dec, and Cen A near 13^h RA and −42° Dec.

9. COMPARISON WITH THE PKSCAT90 DATABASE

The Southern and Tropical PMN Surveys cover a large fraction of the sky previously surveyed with the Parkes and Molonglo telescopes. These earlier surveys were made respectively at 2700 MHz ("The Parkes 2700 MHz Survey," e.g., Bolton *et al.* 1979) and at 408 MHz (*The Molonglo Reference Catalogue of Radio Sources*, Large *et al.* 1981). The 2700 MHz data from the Parkes Survey is contained in the PKSCAT90 database (Wright & Otrupcek 1990) with associated flux information at other radio frequencies, from other observatories, and optical information for the identified objects.

We have compared our new source lists with these older catalogs. As expected, essentially all previously known sources were rediscovered in our surveys. There are a total 7538 sources in the area surveyed listed in either the PKSCAT90 or Molonglo databases. For comparison, the PMN Surveys list 36 640 objects. The new surveys have therefore increased the number of known sources in the Southern and Tropical areas by a factor of about 5. A detailed comparison of the catalogs will form the basis of a future paper.

10. CONCLUSIONS

We have conducted a set of new, deep radio surveys of the southern skies at a frequency of 4850 MHz. At the present time, the Southern ($-87.5° < \delta < -37°$) and Tropical ($-29° < \delta < -9.5°$) Surveys have been fully reduced.

The flux limits of the Southern Survey vary from about 20 mJy near the South celestial pole to about 45 mJy for the less southerly zones. The flux limit for the Tropical Survey is about 42 mJy but increases to 55 mJy near declination −29°. The Tropical source list provides appreciable overlap with the northern-made Condon *et al.* survey and will be valuable for variability work and cross-checking.

Overall, our new source lists increase the number of known southern radio sources in the Southern and Tropical zones by a factor of about 5 over those known previously from the Parkes 2700 MHz and Molonglo 408 MHz surveys.

The source lists resulting from the PMN Surveys will be published in both printed and machine-readable form as they become available and can be obtained either from ATNF headquarters at Epping, Australia, or from MIT, USA on request. In addition, a set of AIPS-readable maps of the PMN data is being produced to facilitate work on sources with extended features.

We have developed a new technique for reducing large-area surveys and determining many of the survey parameters. The false-source injection tests were used to estimate completeness and reliability of the source list, to set the flux limit of the catalog, and to measure biases caused by the reduction process.

Later papers in this series will present the source lists themselves, will discuss the source statistics, and will provide comparisons with objects listed in previous catalogs.

We would like to thank Bernie Burke and Ron Ekers who helped instigate the Parkes–MIT–NRAO Surveys and the large team of staff engineers who made it possible. In particular, George Behrens and Dave Cooke for the receiver installation and Andrew Hunt and Euan Troup for developing much of the telescope control hardware and software. We also must express our appreciation to the large team of observers from most of Australia's astronomical institutions who assisted with the observing shifts over many days. Without them, this work would not have been possible. We are grateful to the MITSF for providing assistance on use of the Cray computer and to the staffs of the ATNF and NRAO for their assistance during these measurements. Finally we thank Sam Conner, André Fletcher, and Jim Condon for helpful comments and advice throughout the course of this work. This work was supported, in part, by a grant from the National Science Foundation.

REFERENCES

Baars J. M. W., Genzel, R., Pauliny-Toth, I. I. K., & Witzel, A. 1977, A&A, 61, 99
Bennett, C. L., Lawrence, C. R., & Burke, B. F. 1985, ApJ, 299, 373
Bolton, J. G., Wright, A. E., & Savage, A. 1979, AuJPA, 46
Condon, J. J., Broderick, J. J., & Seielstad, G. A. 1989, AJ, 97, 1064
Condon, J. J., Broderick, J. J., & Seielstad, G. A. 1991, AJ, 102, 2041
Dickel, H. R., Lortet, M.-C., & de Boer, K. S. 1987, A&AS, 68, 75
Gregory, P. C., & Condon, J. J. 1991, ApJS, 75, 1011
Griffith, M. R. 1993, Ph.D. thesis, Massachusetts Institute of Technology
Griffith, M. R., *et al.* 1991, Proc. Astron. Soc. Australia, 9, 243
Hunt, A., & Wright, A. 1992, MNRAS, 258, 217
Kuhr, H., Witzel, A., Pauliny-Toth, I. I. K., & Nauber, U. 1981, A&AS, 45, 367
Large, M. I., Mills, B., Little, A. G., Crawford, D. F., & Sutton, J. M. 1981, MNRAS, 194, 693
Murdoch, H. S., Crawford, D. F., & Jauncey, D. L. 1973, ApJ, 1973, 183, 1
Stetson, P. B. 1987, PASP, 99, 191
Wright, A. E. 1992, private communication
Wright, A. E., & Otrupcek, R., Eds. 1990, ATNF, PKSCAT90—The Southern Radio Database (available from R. Otrupcek on request in either printed or machine-readable form)